Crystal Structures and Fluorescence Spectroscopic Properties of Cyano-Substituted Diphenylhexatrienes

ARTICLE *in* CRYSTAL GROWTH & DESIGN · JULY 2014

Impact Factor: 4.89 · DOI: 10.1021/cg5009363

4 AUTHORS, INCLUDING:

Yasuo Norikane

National Institute of Advanced Industrial Scie…

33 PUBLICATIONS **453** CITATIONS

SEE PROFILE

CRYSTAL GROWTH & DESIGN

Article

pubs.acs.org/crystal

Crystal Structures and Fluorescence Spectroscopic Properties of Cyano-Substituted Diphenylhexatrienes

Yoriko Sonoda,*[,†] Midori Goto,[‡] Yasuo Norikane,[†] and Reiko Azumi[†]

[†]Electronics and Photonics Research Institute, National Institute of Advanced Industrial Science and Technology (AIST), Higashi 1-1-1, Tsukuba, Ibaraki 305-8562, Japan

[‡]Nanosystem Research Institute, National Institute of Advanced Industrial Science and Technology (AIST), Higashi 1-1-1, Tsukuba, Ibaraki 305-8565, Japan

Supporting Information

ABSTRACT: The crystal structures and spectroscopic properties of (*E*,*E*,*E*)-1,6-di(*x*-cyanophenyl)-1,3,5-hexatrienes (**2**: *x* = 2, **3**: *x* = 3, **4**: *x* = 4) have been investigated. The single crystal X-ray structure analysis reveals that the molecules are linked via sp^2-CH···N≡C hydrogen bonds in each crystal. The existence of the sp^2-CH···N≡C hydrogen bonds in crystals **2**−**4** is spectroscopically evidenced by the fact that the IR peaks due to C≡N stretching vibration shift to lower wavenumbers in the solid state relative to those in solution. The molecules of **3** are hydrogen bonded to form orthogonally oriented ribbons, whereas those of **2** and **4** are organized into molecular sheets. The distance and displacements between the nearest stacking molecules are larger in **3** than those in **2** and **4**. For each triene, the absorption and fluorescence spectra in the solid state shift to longer wavelengths than those in solution. The magnitude of the red shift is similar for **2**−**4** in the absorption spectra, but larger for **2** and **4** than for **3** in the fluorescence spectra. We conclude that the origin of the solid-state fluorescence is monomeric for **3** and excimeric for **2** and **4**. The relationship between crystal structure and fluorescence properties is discussed.

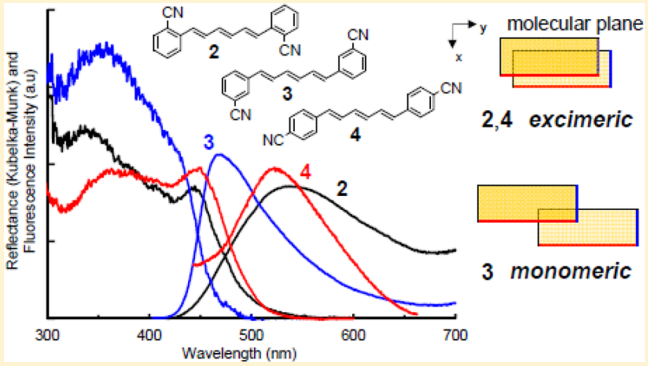

INTRODUCTION

The fluorescence properties of organic molecules in the solid state have long attracted much attention in the field of basic photochemistry,[1,2] and have also been intensively studied recently in the field of material chemistry. At present, many conjugated molecules and polymers have been developed for use in light-emitting devices such as organic light emitting diodes (OLEDs) and organic solid lasers.[3−8]

Fluorescence emission from excimeric species is one of the main photoprocesses in organic solids.[1,2] Although excimer formation often results in a large decrease in fluorescence yields, a number of recent studies have shown that the red-shifted emission from excimers can effectively be used for fluorescence tuning.[8−11]

As the crystal structures strongly affect the solid-state emission properties, an understanding of the structure−property relationship in the solid state is very important not only in basic photochemistry, but also in material chemistry. However, the structure−property relationship in the solid state is much more complex relative to that in solution, and has not been fully understood yet. Despite the numerous intensive studies during the past years, it is still difficult to understand the direct correlation between mutual molecular arrangements in crystals and the resulting solid-state photoproperties.[7,8] As pointed out by Gierschner et al., this is mainly because the solid-state photoproperties are determined not only by intramolecular factors such as the nature of the molecular backbone, effective conjugation, substituent pattern, and sterical demands, but also by intermolecular factors.[8a]

For a better understanding of the structure−property relationship in organic solids, a systematic study on the substituent effects on the emission properties of molecules is required. The introduction of substituents into the double bonds or phenyl rings of 1,4-distylylbenzene[6−8,12] and higher phenylenevinylene oligomers,[4] for example, leads to large changes in solid-state spectroscopic properties. In particular, the introduction of cyano groups has proven to be very effective to improve the emission properties of these molecules.[4−6,8,9,13,14] The improvements should at least partially be due to the changes in molecular arrangements in crystals or solids, resulting from the changes in intermolecular interaction induced by the cyano substitution.

(*E*,*E*,*E*)-1,6-Diphenyl-1,3,5-hexatriene (DPH) (**1**, Chart 1) is a highly fluorescent molecule with a one-dimensional polyenic structure. DPH is known for its potentially rare and unusual photophysical properties in solution; it exhibits dual

Received: June 27, 2014
Revised: July 24, 2014
Published: July 30, 2014

Chart 1. Chemical Structures of 1−4

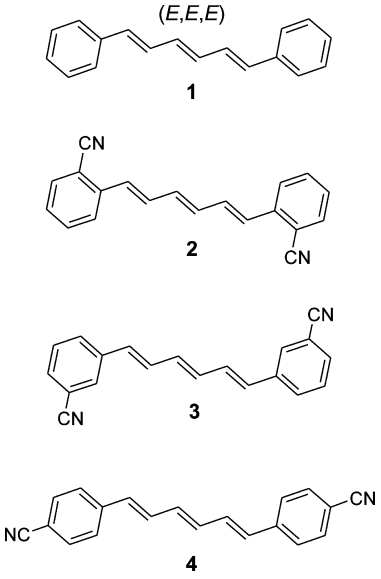

fluorescence from the first two singlet excited states, S_1 and S_2, to the ground state, S_0.[15,16] Further, DPH and its derivatives are also useful as fluorescence probes and imaging agents in biochemical and medicinal studies.[17]

As for the emission properties of DPHs in the solid state, we showed that the unsubstituted parent compound **1** exhibited measurable fluorescence in the thin film and microcrystalline state.[18] For over a decade, we have investigated the crystal structures and solid-state fluorescence properties of symmetric[18−22] and asymmetric[23] DPH derivatives having various kinds of ring-substituents. For the asymmetrically substituted 4-alkoxy-4′-nitro-DPHs (alkoxy = methoxy, ethoxy, propoxy, and butoxy), for example, the absorption and fluorescence properties in diluted solution (i.e., the properties of isolated molecules) are the same regardless of the alkoxy chain length.[23] In contrast, the solid-state spectroscopic properties are clearly different depending on the chain length. The absorption and fluorescence spectra of the ethoxy and butoxy derivatives are red-shifted relative to those of the methoxy and propoxy derivatives. This can be attributed to the difference in molecular packing pattern in crystals: π-stacked (the ethoxy and butoxy derivatives) vs herringbone (the methoxy and propoxy derivatives). The intermolecular orbital−orbital interaction is expected to be stronger in the π-stacked crystal structure than in the herringbone one.

Herein we report the crystal structures and solid-state absorption and fluorescence properties of 2,2′-, 3,3′-, and 4,4′-dicyano-substituted DPHs (**2**, **3**, and **4**, respectively) as shown in Chart 1. Compounds **2** and **3** were newly prepared in this study. As for **4**, we have briefly reported that the fluorescence spectrum in the solid state shifts largely to longer wavelengths than that in solution.[24] The strongly red-shifted fluorescence should be related with the pattern of molecular arrangements in the solid state; however, the single-crystal structure analysis of **4** was previously unsuccessful.[24,25]

EXPERIMENTAL SECTION

Materials. HR-MS data were obtained using a Hitachi M80B spectrometer. ^{1}H and ^{13}C NMR spectra were recorded on a BRUKER AVANCE 500 (500.13 and 125.77 MHz, respectively) with tetramethylsilane (TMS) as internal reference. Cyanobenzaldehydes and (*E*)-2-butene-1,4-bis(triphenylphosphonium chloride) were purchased from WAKO and TCI, respectively, and used without further purification. All the solvents used in the absorption, fluorescence, and FT-IR measurements were of spectroscopic grade (Dojin).

(*E,E,E*)-1,6-Di(2-cyanophenyl)-1,3,5-hexatriene (2). To a solution of 2-cyanobenzaldehyde (1.31 g, 10 mmol) and (*E*)-2-butene-1,4-bis(triphenylphosphonium chloride) (3.25 g, 5 mmol) in ethanol (13 mL) was slowly added a solution of sodium ethoxide in ethanol (0.30 M, 34 mL) at 50 °C under nitrogen atmosphere. After stirring for 24 h, water (30 mL) was added to the reaction mixture and the solution was vigorously stirred for 60 min. The resulting pale yellow precipitate was filtered off, washed twice with aqueous ethanol (60% v/v, 20 mL) and twice with water (20 mL), and dried under vacuum at room temperature. The crude product (*Z*-*E* mixture) was irradiated for 4 h in toluene with Pyrex-filtered light at room temperature in air to induce *Z*-to-*E* isomerization. A 500 W high-pressure mercury lamp was used as a light source. After the irradiation, the solvent was evaporated and the resulting yellow solid (predominantly *E,E,E*) was recrystallized from toluene. The purity was checked by HPLC. The single crystals of **2** suitable for X-ray analysis were grown from a solution of the recrystallized product in acetonitrile by very slow evaporation of the solvent at room temperature in the dark. Mp 218−220 °C. HR-MS Found: 282.1132, Calcd for $C_{20}H_{14}N_2$: 282.1157. ν_{max} (KBr) 2216, 1591, 1479, 1293, 1000, 957, 925, 852, 764, 758, and 747 cm^{-1}. ^{1}H NMR ($CDCl_3$) δ 7.73 (2H, d, J = 8.0 Hz, arom.), 7.63 (2H, d, J = 7.8 Hz, arom.), 7.56 (2H, t, J = 7.5 Hz, arom.), 7.31 (2H, t, J = 7.6 Hz, arom.), 7.07 (2H, ddd, J = 15.4, 6.1, and 2.9 Hz, triene), 7.01 (2H, d, J = 15.4 Hz, triene), and 6.69 (2H, dd, J = 6.2 and 2.9 Hz, triene). ^{13}C NMR ($CDCl_3$) δ 140.2, 135.3, 133.1, 132.9, 132.7, 129.2, 127.7, 125.1, 117.9, and 111.1. UV−vis λ_{max} (acetonitrile) 368 nm (ε = 66 600 M^{-1} cm^{-1}).

(*E,E,E*)-1,6-Di(3-cyanophenyl)-1,3,5-hexatriene (3). Triene **3** was prepared and purified by a similar procedure described for **2**. Mp 223−225 °C. HR-MS Found: 282.1147, Calcd for $C_{20}H_{14}N_2$: 282.1157. ν_{max} (KBr) 2226, 1591, 1575, 1480, 1424, 1175, 992, 979, 916, 902, 790, and 680 cm^{-1}. ^{1}H NMR ($CDCl_3$) δ 7.69 (2H, s, arom.), 7.63 (2H, d, J = 7.6 Hz, arom.), 7.51 (2H, d, J = 7.6 Hz, arom.), 7.43 (2H, t, J = 7.6 Hz, arom.), 6.93 (2H, ddd, J = 15.4, 7.0, and 2.7 Hz, triene), 6.60 (2H, d, J = 15.8 Hz, triene), and 6.58 (2H, dd, J = 6.6 and 3.3 Hz, triene). ^{13}C NMR ($CDCl_3$) δ 138.4, 134.4, 131.1, 131.0, 130.8, 130.4, 129.7, 129.5, 118.7, and 113.0. UV−vis λ_{max} (acetonitrile) 356 nm (ε = 69 700 M^{-1} cm^{-1}).

(*E,E,E*)-1,6-Di(4-cyanophenyl)-1,3,5-hexatriene (4). Triene **4** was prepared and purified by a similar procedure described for **2**. Mp 245−247 °C (lit.[26] 235 °C). ν_{max} (KBr) 2222, 1600, 1506, 1174, 1001, 874, and 816 cm^{-1}. The ^{1}H NMR data have already been described.[27] ^{13}C NMR ($CDCl_3$) 141.5, 134.9, 132.5, 132.1, 131.9, 126.8, 119.0, and 110.7. UV−vis λ_{max} (acetonitrile) 375 nm (ε = 79 200 M^{-1} cm^{-1}).

Single Crystal X-ray Structure Analyses. The single crystal X-ray diffraction measurements of **2**−**4** were performed at −90 °C using a Bruker SMART CCD area-detector diffractometer with graphite monochromated Mo Kα radiation (λ = 0.71073 Å). Data collection, reduction, and empirical absorption correction were carried out using APEX II, SAINT, and SADABS.[28] The structure was solved by direct methods and refined by full matrix least-squares on F^2 with SHELXTL.[29] The non-hydrogen atoms were refined anisotropically. Hydrogen atoms were placed in geometrically calculated positions and refining a riding model.

Measurements of FT-IR Spectra. The FT-IR spectra of **2**−**4** in carbon tetrachloride were measured at room temperature in air using a JASCO FT/IR-420 spectrometer. The sample solutions were placed between two KBr plates of a sample holder for liquid measurements. Typically, 16 scans were collected at a resolution of 4 cm^{-1}. The spectra for the KBr pellet samples were measured using a Mattson Infinity Gold FT-IR spectrometer with 8 scans at a resolution of 4 cm^{-1}. The errors were estimated to be 1 cm^{-1}.

Measurements of Absorption, Fluorescence and Fluorescence Excitation Spectra, Fluorescence Lifetimes, and Quantum Yields. The absorption spectra of **2**−**4** in solution were measured at room temperature in air using a Shimadzu UV-3150

dx.doi.org/10.1021/cg5009363 | Cryst. Growth Des. 2014, 14, 4781−4789

spectrometer. For the measurements in diluted solution, the concentration of the sample was (1−3) × 10^{-5} M, and the optical density (OD) at the absorption maximum wavelength (λ_a) was set at 1.0−1.5. For the measurements in concentrated solution, the sample concentration was (2−3) × 10^{-3} M. The absorption spectra in the solid state were obtained by Kubelka−Munk conversion of diffuse reflectance spectra. The reflectance spectra were recorded on a Shimadzu UV-3150 spectrometer equipped with an integrating sphere accessory (model ISR-3100). The corrected fluorescence and fluorescence excitation spectra of **2**−**4** in solution and in the solid state were measured at room temperature in air using a Hitachi F-7000 spectrometer. For the measurements in diluted solution, the sample concentration was (1−2) × 10^{-6} M, and the OD at the excitation wavelength (λ_{ex} = 360 nm) was set at <0.1 to avoid reabsorption. The fluorescence and fluorescence excitation spectra of the concentrated solution and solid samples were recorded using the front face geometry. The fluorescence decay curves and lifetimes (τ_s) were measured at room temperature in air by the time-correlated single-photon counting (TCSPC) method, using a Hamamatsu Photonics C11367 equipped with UV LEDs (λ_{ex} = 365 nm) (time resolution better than 100 ps). The emission (monitor) wavelengths (λ_{em}) are shown in Tables 4, 5, and S2−S4 and S6 (Supporting Information). The fluorescence quantum yields (ϕ_f) in diluted solution were determined at room temperature in air, using **4** in toluene as the standard (ϕ_f = 0.88).[27] The solid-state ϕ_f were measured using a Hamamatsu Photonics C11347 (λ_{ex} = 360 nm).

For the measurements of absorption and fluorescence spectra, τ_s, and ϕ_f, quartz cells of 10 mm and 2 mm path lengths were used for the diluted and concentrated solution samples, respectively. All solid-state spectroscopic measurements were performed for microcrystalline samples, which were obtained by manual grinding (crushing) some of the grown crystal blocks. For the measurements of absorption and fluorescence spectra and τ_s, the microcrystalline samples were placed between quartz plates (40 × 10 mm^2). The sample thickness was estimated to be 0.025−0.050 mm. For the measurements of ϕ_f, the samples were encapsulated in quartz cells (ϕ 15 mm × 5 mm).

Computational Method. Theoretical calculations were performed using the GAUSSIAN 09W program package.[30] The B3LYP[31] method was employed with 6-31G(d,p) basis set for geometrical optimizations, vibration frequency calculations, and time-dependent DFT (TD-DFT)[32] calculations. Molecular structure was fully optimized by using crystal structure as an initial structure. The optimized structures had no imaginary frequencies. Excitation energies and ground-to-excited state transition electric dipole moments were calculated by the TD-DFT calculation with the consideration of lowest 30 transitions (N_{states} = 30).

RESULTS AND DISCUSSION

1. Crystal Structures. Table 1 shows the single crystal data of **2**−**4** obtained by X-ray structure analyses. The ORTEP drawings are shown in Figures S1−S3 in Supporting Information (SI).

1.1. Molecular Structures. The major geometrical parameters are summarized in Table S1 (SI). In each crystal, there exist two crystallographically independent molecules, A and B, in a unit cell. Each molecule has a center of symmetry. The lengths of the C−C single and C═C double bonds in the triene and the bond length alternation (BLA) are similar for **2**−**4**. The molecules of **2**−**4** are fundamentally planar. The deviations from the least-squares planes (LSP) defined by all non-hydrogen atoms (C1−C10 and N1) are less than 0.06 Å, and the torsion angles C6−C1−C7−C8 (Ar−CH) are smaller than 16°. The Ar−CH torsion angles in **2** can be compared with the values in 2,2′-dinitro- (19.9° and 23.4°)[20] and 2,2′-dimethoxy-substituted (15.6°)[33] DPHs.

1.2. Molecular Arrangements. In the crystal of **2**, molecules A and B are linked with each other via the CH···N-type hydrogen bonds (Figure S1(b), Supporting Information). Table 2a summarizes the hydrogen bond geometries. The distances between the nitrogen and hydrogen atoms (d(N···H)) are slightly but clearly less than the sum of the van der Waals radii of 2.80 Å.[34−36] These hydrogen bonds are bifurcated,[37,38] although some of them have relatively small C−H···N angles (∠C−H···N). We note that the CH···N hydrogen bonds are only formed between A and B, and not found between the two molecules of A, or between those of B. The molecules are hydrogen bonded to form a two-dimensional sheet structure, although the planarity is not very high. For the neighboring four molecules of A1, A2 and B1, B2 shown in Figure S1(b), the dihedral angles between the LSPs of

Table 1. Crystal Data of 2−4

	2	3	4
formula	$C_{20}H_{14}N_2$	$C_{20}H_{14}N_2$	$C_{20}H_{14}N_2$
formula weight	282.34	282.34	282.34
crystal color, habit	colorless, needle	colorless, rectangular	pale yellow, plate
crystal size (mm^3)	0.60 × 0.05 × 0.05	0.45 × 0.10 × 0.05	0.40 × 0.10 × 0.03
crystal system	monoclinic	triclinic	triclinic
space group	$P2_1/n$	$P\bar{1}$	$P\bar{1}$
a (Å)	18.460(7)	5.481(2)	3.9187(3)
b (Å)	4.040(2)	12.043(3)	11.905(1)
c (Å)	19.941(7)	12.301(4)	16.255(1)
α (deg)	90	71.769(3)	100.980(1)
β (deg)	91.544(4)	79.633(3)	91.214(1)
γ (deg)	90	78.979(3)	94.833(1)
V ($Å^3$)	1486.7(9)	750.6(4)	741.3(1)
Z	4	2	2
D_{calc} (g/cm^3)	1.261	1.249	1.265
T (°C)	−90(2)	−90(2)	−90(2)
mp (°C)	220	225	247
R_1 (I > 2σ(I))	0.0506	0.0333	0.0368

Table 2. Hydrogen Bond Lengths and Angles in 2−4

(a) Crystal **2**				
C−H···N	d(C−H)[a]	d(N···H)[a]	d(N···C)[a]	∠C−H···N[b]
C4B−H4B^{i}···N1A	0.95	2.75	3.417(3)	128.3
C6B−H6B^{ii}···N1A	0.95	2.75	3.686(4)	169.1
C4A−H4A^{iii}···N1B^{iv}	0.95	2.68	3.361(4)	129.1
C6A−H6A···N1B^{iv}	0.95	2.69	3.550(4)	151.5
Symmetry codes: (*i*) x+1, y+1, z, (*ii*) −x+(3/2), y+(3/2), −z+(3/2), (*iii*) −x +(1/2), y+(1/2), −z+(3/2), (*iv*) −x+1, −y+1, −z+2.				
(b) Crystal **3**				
C−H···N	d(C−H)[a]	d(N···H)[a]	d(N···C)[a]	∠C−H···N[b]
C4A−H4A^{i}···N1A	0.95	2.54	3.425(2)	154.4
C6B−H6B^{ii}···N1B	0.95	2.51	3.442(2)	166.3
C8B−H8B^{ii}···N1B	0.95	2.74	3.675(2)	166.7
Symmetry codes: (*i*) −x+3, −y+1, −z+1, (*ii*) −x+1, −y+1, −z.				
(c) Crystal **4**				
C−H···N	d(C−H)[a]	d(N···H)[a]	d(N···C)[a]	∠C−H···N[b]
C3A−H3A^{i}···N1A	0.95	2.72	3.475(2)	137.0
C3B−H3B^{ii}···N1B	0.95	2.59	3.487(2)	158.4
C7A−H7A···N1B^{ii}	0.95	2.70	3.644(2)	174.7
Symmetry codes: (*i*) 2−x, 1−y, 1−z, (*ii*) −x, 1−y, −z.				

[a] d: distance in Å. [b] Angle in °. For atom numbering, see Figures S1(a), S2(a), and S3(a) in Supporting Information.

dx.doi.org/10.1021/cg5009363 | Cryst. Growth Des. 2014, 14, 4781−4789

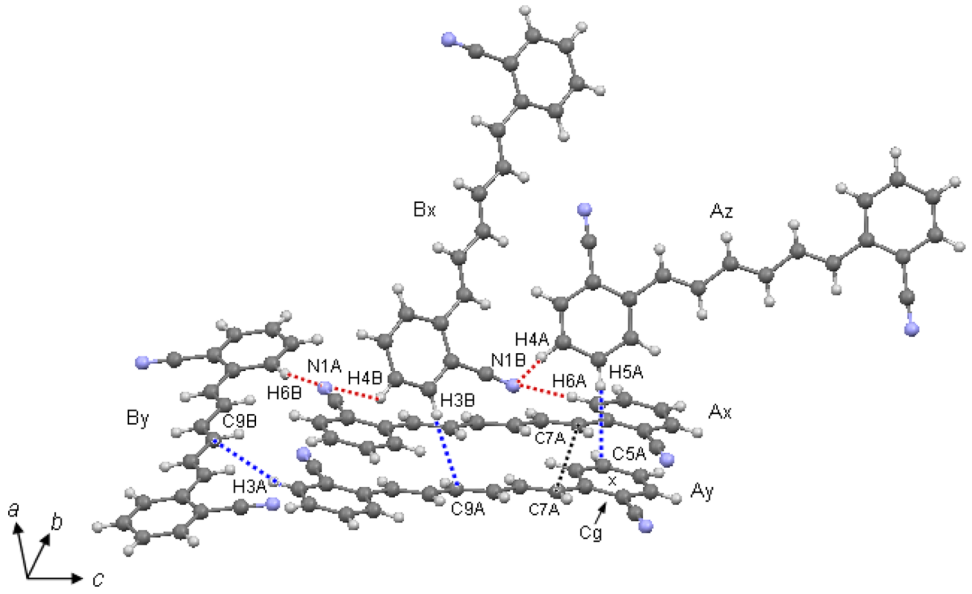

Figure 1. Crystal packing diagram of **2**. The CH···N and CH···π interactions are shown as red and blue dotted lines, respectively. Cg: center of gravity.

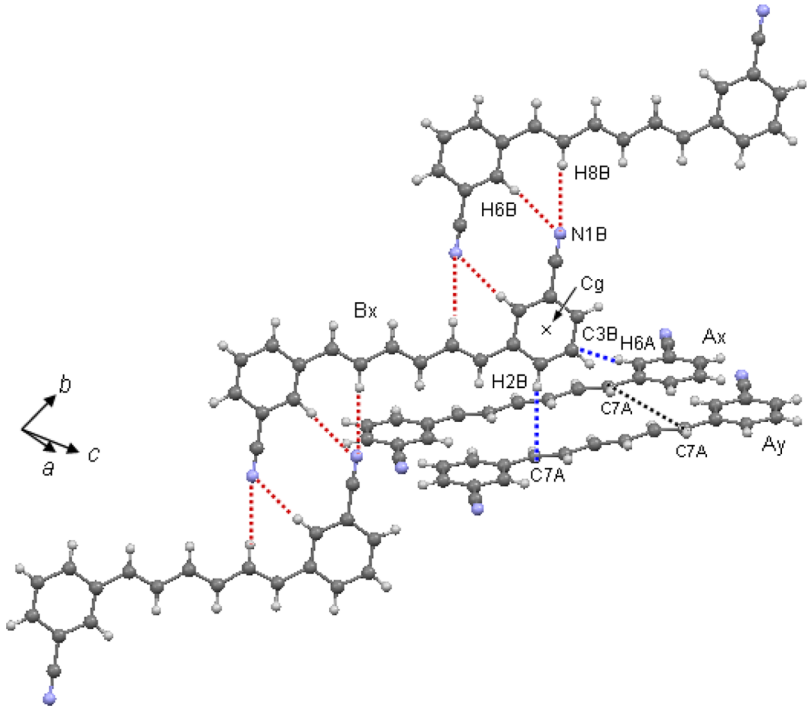

Figure 2. Crystal packing diagram of **3**. The CH···N and CH···π interactions are shown as red and blue dotted lines, respectively. Cg: center of gravity.

the molecules are 63.33(4)° for A1 and A2, 62.80(3)° for B1 and B2, 58.16(4)° for A1 and B1, and 22.26(3)° for A1 and B2. Figure 1 shows the partial crystal structure of **2**. In the Figure, molecules A*x* and B*x* are linked via the CH···N hydrogen bonds as described above. Molecule B*x* is also in close proximity to molecule A*y*, which is shown below A*x* along the *b* axis. The intermolecular distance between the olefinic C9A (x, y+1, z) of A*y* and the aromatic H3B (x+1, y+1, z) of B*x* is 2.71 Å. This proximity may at least partially be due to the CH···π-type interaction.[39] Similarly, the distance between the olefinic C9B (x+0.5, −y+1.5, z−0.5) of molecule B*y* and the aromatic H3A (x, y+1, z) of A*y* is 2.86 Å. The distance of the aromatic C5A (2−x, 3−y, 2−z) of A*y* and the aromatic H5A (x+0.5, −y+2.5, z +0.5) of molecule A*z* is also relatively short (2.83 Å), although the distance between the center of gravity of the benzene ring (shown as Cg in Figure 1) of A*y* and H5A of A*z* is considerably long (3.65 Å). The shortest intermolecular distance between the olefinic C7A of the stacking molecules of A*x* and A*y* is determined by all these interactions to be 4.040(2) Å (=*b*) in the structure.

In the crystal of **3**, two molecules of A are CH···N hydrogen bonded to form a planar ring structure (Figure S2(b), Supporting Information). A similar ring structure is formed by the two hydrogen-bonded molecules of B. In this case, the

dx.doi.org/10.1021/cg5009363 | *Cryst. Growth Des.* 2014, 14, 4781−4789

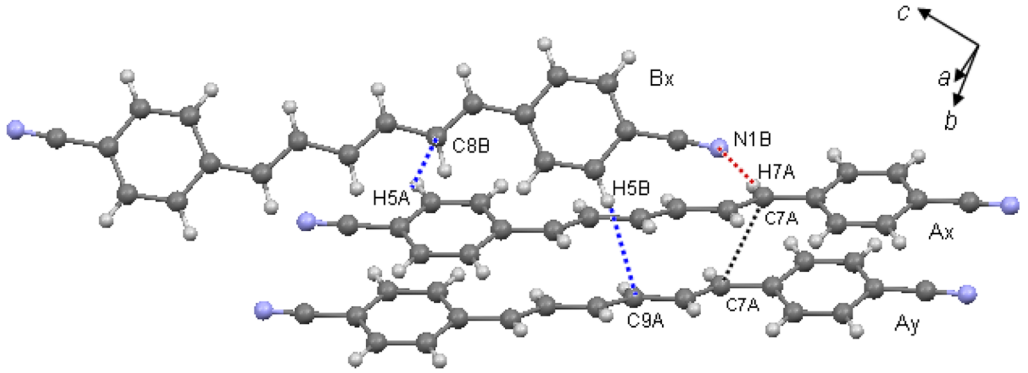

Figure 3. Crystal packing diagrams of **4**. The CH···N and CH···π interactions are shown as red and blue dotted lines, respectively.

aromatic H6B and olefinic H8B are both involved in the CH···N hydrogen bonding. Table 2b summarizes the hydrogen bond geometries for **3**. In the crystal, d(N···H) are clearly shorter than the sum of the van der Waals radii of 2.80 Å[36] and ∠C−H···N are all larger than 150°. This suggests the existence of considerably strong CH···N interactions. In **3**, the CH···N hydrogen bonds are only formed between molecules A and between molecules B, and not found between A and B. The infinite chains of the ring structures of hydrogen-bonded molecules A, and those of B, form one-dimensional ribbons of A and B, respectively. These molecular ribbons are nearly orthogonally oriented, as shown in Figure S2(c) (Supporting Information). The dihedral angle between the LSPs of A and B is 81.61(2)°. Figure 2 shows the partial crystal structure of **3**. The relatively short distance of 2.76 Å between the aromatic H2B (x, y, z) of molecule Bx and the olefinic C7A (2−x, −y, 1−z) of molecule Ay is possibly due to the CH···π interaction. Similarly, the distance of the aromatic H6A (x, y, z) of Ax and the aromatic C3B (x, y, z) of Bx is relatively short (2.86 Å), although the distance of H6A of Ax and the center of gravity of the benzene ring (shown as Cg in Figure 2) of Bx is considerably long (3.58 Å). The distance between the olefinic C7A of the stacking molecules of Ax and Ay is 5.481(2) Å (=a).

As in **3**, the two molecules of A in crystal **4** are CH···N hydrogen bonded to form a planar ring structure (Figure S3(b), Supporting Information). From the hydrogen bonded molecules of B, the ring structures are similarly formed. The infinite chains of the ring structures of A and B form molecular ribbons of A and B, respectively. Unlike in **3**, however, the CH···N hydrogen bonds are not only formed between molecules A, and between molecules B, but also formed between A and B. Thus, the one-dimensional ribbons A and B in **4** are further linked by the CH···N hydrogen bonds between molecules A and B to form a two-dimensional sheet. The dihedral angle between the LSPs of A and B is 43.51(4)°. Table 2c summarizes the hydrogen bond geometries for **4**. In the crystal, d(N···H) are significantly shorter than the sum of the van der Waals radii (2.80 Å),[36] and ∠C−H···N are relatively large. Figure 3 shows the partial crystal structure of **4**. Molecules Ax and Bx in the figure are linked by the CH···N hydrogen bonds as described above. For this pair, the distance between the aromatic H5A (−x, −y, −z) of Ax and the olefinic C8B (−x, −y+1, −z) of Bx is also relatively short (2.83 Å). Further, Bx is in close proximity to molecule Ay, which is shown below Ax along the a axis. The short distance of 2.72 Å between the aromatic H5B (−x, −y+1, −z) of Bx and the olefinic C9A (x+1, y, z) of Ay possibly results from the CH···π interaction. The distance between the olefinic C7A of the two stacking molecules of Ax and Ay is 3.9187(3) Å (=a) in **4**.

1.3. CH···N Hydrogen Bonds. The CH···N≡C hydrogen bonding would be one of the most important forces to determine the crystal structures of cyano molecules.[40−45] This type of hydrogen bond is seen in the structures of benzonitrile;[46] 1,2-, 1,3-, and 1,4-dicyanobenzenes;[40,42,47−49] 1,3,5-tricyanobenzene;[41,44,50,51] 3- and 4-cyano-cinnnamic acids;[52] and others.[53−56] Among them, the ring structures similar to those observed in the crystals of **3** and **4** are also described for dicyanobenzenes[40,42,47−49] and cyano-cinnnamic acids.[52] In these structures, the rings are considered to be (further) stabilized by the CN···CN dipole−dipole (electrostatic) interaction.[52,57,58] In crystal **3**, the intermolecular distance between C10A and N1A in the CH···N ring is 3.630(2) Å, and that between C10B and N1B in the ring is 4.038(2) Å (the green dotted lines in Figure S2(b), Supporting Information). In **4**, the distance of C10A and N1A and that of C10B and N1B are 3.401(2) Å and 3.764(2) Å, respectively (the green dotted lines in Figure S3(b), Supporting Information). These values are not greatly different from the corresponding distances of 3.626 Å in 1,4-dicyanobenzene[58] and 3.47−3.48 Å in 3- and 4-cyano-cinnamic acids.[52]

To obtain spectroscopic evidence for the CH···N≡C hydrogen bonds in crystals **2**−**4**, FT-IR spectra were measured in solution and in the solid state. If hydrogen bond formation leads to a large change in electron density in the C≡N triple bond, it should be coupled with a measurable spectral shift. Table 3 summarizes the frequencies of the C≡N stretching

Table 3. IR Frequencies of C≡N Stretching Vibration of 2−4[a]

	2	3	4
Solution[b]	2225	2232	2226
Solid[c]	2216	2226	2222

[a]In cm^{-1}. [b]In carbon tetrachloride. [c]KBr pellet.

vibration of cyano groups (ν_{CN}) for the diluted solutions in carbon tetrachloride and for the KBr pellet samples of **2**−**4**. In all cases, the ν_{CN} peaks shift to lower wavenumbers in the solid state than those in diluted solution. For more concentrated (almost saturated) solutions, two peaks are occasionally observed, whose frequencies are the same as those in diluted solution and in the solid state. The IR spectra of **2**−**4** in the ν_{CN} region are displayed in Figures S4−S6 (Supporting Information). The red shifts of the ν_{CN} peaks in the solid state should result from the fact that the formation of hydrogen bond

dx.doi.org/10.1021/cg5009363 | Cryst. Growth Des. 2014, 14, 4781−4789

induces the lengthening (weakening) and polarization of the C≡N triple bond, and thus provide clear evidence for the fact that the nitrogen atoms of the cyano groups serve as the CH···N hydrogen bond acceptors in crystals **2**–**4**. The ability of sp^2-CH groups to donate hydrogen bonds is in general considered to be weak relative to that of sp-CH.[43,45] This can clearly be seen in the fact that d(N···H) in **2**–**4**, where all hydrogen bonds are sp^2-CH···N, are considerably longer than the typical value of 2.35 Å for the sp-CH···N hydrogen bonds[36] (Table 2). It would therefore be valuable that the existence of such weak sp^2-CH···N≡C hydrogen bonds is spectroscopically evidenced in the crystals of **2**–**4**. To the best of our knowledge, very few examples have been reported for the shifts in ν_{CN} due to the formation of sp^2-CH···N≡C hydrogen bonds in crystals so far.

We can compare the present observation with that for 1,6-bis(4-formylphenyl)-1,3,5-hexatriene, which we reported previously.[59] The aldehyde molecules are sp^2-CH···O=C hydrogen bonded in the crystal, as shown by the X-ray structure analysis. In this case, the IR peak due to the C=O stretching vibration of the formyl group shifts from 1702 cm^{-1} in solution to 1684 cm^{-1} in the solid state. Thus, although the magnitude of the peak shift is somewhat larger for the CH···O hydrogen bonds in the formyl derivative than that for the CH···N hydrogen bonds in **2**–**4**, the directions of the shifts are the same in these cases.

2. Absorption and Fluorescence Spectroscopic Properties. *2.1. Properties in Solution.* Figures 4 and S7 (Supporting Information) show the absorption and fluorescence spectra for the diluted solutions of **2**–**4** in low polarity methylcyclohexane and higher polarity acetonitrile, respectively. The spectroscopic data are summarized in Tables 4 and S2–S4 (Supporting Information).

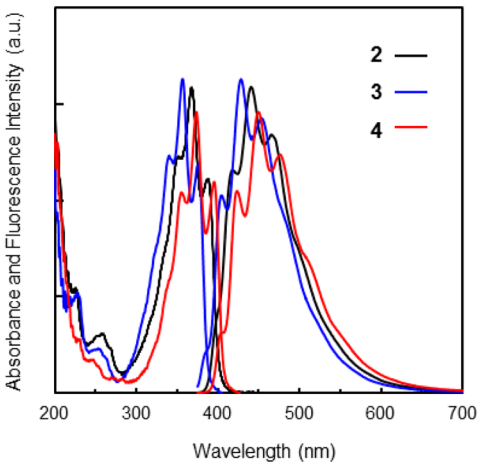

Figure 4. Absorption and fluorescence spectra of **2**–**4** in methylcyclohexane. The spectra are normalized for each molecule. Excitation wavelength: λ_{ex} = 360 nm.

The absorption spectra of **2**–**4** in methylcyclohexane similarly show vibrational structures. The energy spacings of the structures are about 1400 cm^{-1}. Although the value is similar to the frequency of C=C stretching vibration of conjugated trienes, this assignment is probably oversimplified. At room temperature, inhomogeneous spectral broadening often leads to an 'apparent' single vibronic structure, which nevertheless consists of several modes.[60] The spectra shift to longer wavelengths in the following order, **3** → **2** → **4**. The energy difference between the absorption maxima (λ_a) of **3** and **2** and that of **2** and **4** are relatively small (500–800 cm^{-1}) (Table 4).

Table 4. Absorption and Fluorescence Data of 2–4 in Methylcyclohexane

	2	3	4
λ_a [a]	368 (2.72 × 10^4)	357 (2.80 × 10^4)	374 (2.67 × 10^4)
λ_f [b]	441 (2.27 × 10^4)	428 (2.34 × 10^4)	450 (2.22 × 10^4)
ΔE_{ss} [c] (cm^{-1})	4.5 × 10^3	4.6$_5$ × 10^3	4.5 × 10^3
ϕ_f [d]	0.73	0.61	0.63
τ_s [e] (ns)	6.4	7.6	7.5
k_f [f] (s^{-1})	1.2 × 10^8	8.0 × 10^7	8.3 × 10^7
k_{nr} [g] (s^{-1})	4.2 × 10^7	5.2 × 10^7	5.0 × 10^7

[a]Absorption maxima in nm. Values in parentheses are in cm^{-1}. [b]Fluorescence maxima in nm. Values in parentheses are in cm^{-1}. Excitation wavelength: λ_{ex} = 360 nm. [c]Stokes shifts calculated from λ_a and λ_f. [d]Fluorescence quantum yields. ±10%. [e]Fluorescence lifetimes. Excitation wavelength: λ_{ex} = 365 nm. Emission (monitor) wavelength: λ_{em} = λ_f. [f]Radiative rate constants: k_f = ϕ_f/τ_s. [g]Nonradiative rate constants: k_{nr} = $(1-\phi_f)/\tau_s$.

To understand the electronic transitions responsible for the absorption bands of **2**–**4**, the vertical excitation energies were calculated at the TD-B3LYP/6-31G(d,p)//B3LYP/6-31G(d,p) level. The results are summarized in Table S5 (Supporting Information). The lowest excitation energies from S_0 are calculated to be 406 nm (S_1) for **2**, 387 nm (S_1) for **3**, and 416 nm (S_1) for **4**, and the main configurations of the S_1 states are the HOMO → LUMO transitions for all. The calculated excitation energies are in fairly good agreement with the experimental values of λ_a in methylcyclohexane. The energy ordering of λ_a for **2**–**4** can successfully be reproduced. Thus, the observed red shifts of the spectra in the order of **3** → **2** → **4** actually agree with the expectations of the mesomeric effects when going from 3- → 2- → 4-positions of substitutions. We also performed TD-DFT calculations to determine the orientation of the S_0 → S_1 (HOMO → LUMO) transition dipole moments of **2**–**4**, using the same functional (B3LYP) and basis set (6-31G(d,p)). As seen in Figure S8 (Supporting Information), the transition dipole moments point along the long molecular axes in all three molecules, as in the case of the unsubstituted DPH.[62]

The fluorescence spectra of **2**–**4** also show vibrational structures with energy spacings of about 1300 cm^{-1} in methylcyclohexane. For each molecule, the fluorescence spectrum is nearly the mirror image of the absorption spectrum.[63] The mirror image relation indicates similar torsional potentials in the S_0 and S_1 states.[61] The spectra move to longer wavelengths in the order of **3** → **2** → **4**. The energy difference between the emission maxima (λ_f) of **3** and **2** and that of **2** and **4** are relatively small (500–700 cm^{-1}) (Table 4), similar to the observation in the absorption spectra. As a result of this, the Stokes shifts (ΔE_{ss}) calculated from λ_a and λ_f are similar for **2**–**4** (Table 4). The fluorescence excitation spectra of **2**–**4** are almost independent of λ_{em}, and are fundamentally the same as the absorption spectra. This confirms the validity of Kasha's rule (emission occurs from S_1).[64]

The fluorescence decay curves of **2**–**4** are able to be fitted by monoexponential function to give similar τ_s of 6–8 ns in methylcyclohexane (Table 4). The values are nearly independent of λ_{em}. The results suggest that only one kind of excited-state species is responsible for the emission process of each

dx.doi.org/10.1021/cg5009363 | Cryst. Growth Des. 2014, 14, 4781–4789

molecule. Considering that all solutions are highly diluted and molecules are thus nearly completely isolated, the emission is most probably of monomeric origin. In methylcyclohexane, ϕ_f and τ_s are similar for **2**–**4**, and their radiative rate constants ($k_f = \phi_f/\tau_s$) are therefore not very different (Table 4).

SI Tables S2–S4 collect the absorption and fluorescence data of **2**–**4** in various kinds of solvents with different polarity. For each molecule, λ_a and λ_f do not largely depend on the polarity of solvent. On the other hand, ϕ_f dramatically decreases and τ_s is considerably shortened as the solvent polarity increases. The solvent effects are more strongly observed in **2** and **4** than in **3**. This results in the large differences in ϕ_f and τ_s for **2**–**4** in polar solvents such as methanol, in contrast to the small differences in low polarity methylcyclohexane. If we consider the values of k_f, however, they are not greatly different for **2**–**4** even in methanol solvent. The fact that k_f is hardly changed by the solvent polarity is reasonably expected, since the nature of the transition is essentially preserved (Strickler–Berg relation).[65] As the integrated intensity of the absorption is expected to be not greatly different in each solvent, the small solvent dependence of k_f suggests that the molecular geometry does not change largely upon excitation. In contrast, the nonradiative rate constant ($k_{nr} = (1-\phi_f)/\tau_s$) strongly increases with the increase in solvent polarity (SI Tables S2–S4). Thus, the solvent polarity mainly changes the internal conversion processes, the pathway toward the conical intersection.

We also measured the absorption and fluorescence spectra and τ_s of **2**–**4** in concentrated solution, and compared them with those in diluted solution. Although the fluorescence intensity in shorter wavelengths slightly decreased due to reabsorption, no significant changes were observed in the peak positions or spectral shapes at least in the concentration range we examined. The τ_s values are fundamentally the same as those in diluted solution. Thus, although the existence of CH···N hydrogen bonds in crystal is spectroscopically evidenced by the IR peak shifts as described above, the formation of molecular aggregates is not observable in the absorption and/or fluorescence spectra, even in almost saturated solution.

2.2. Properties in the Solid State. Figure 5 shows the absorption and fluorescence spectra of **2**–**4** in the solid state. The spectroscopic data are summarized in Table 5.

The absorption spectra of **2**–**4** are similarly broad. No vibrational structures are observed at least for the lowest energy bands around 440 nm. The spectra move to longer wavelengths in the following order, **3** → **2** → **4**. Although the assignments of λ_a are rather difficult for optically dense samples like the thick microcrystalline solids of **2**–**4** used in this study (see Experimental Section),[66] the energy difference in λ_a for **3** and **2** and that for **2** and **4** seem to be relatively small (Table 5).

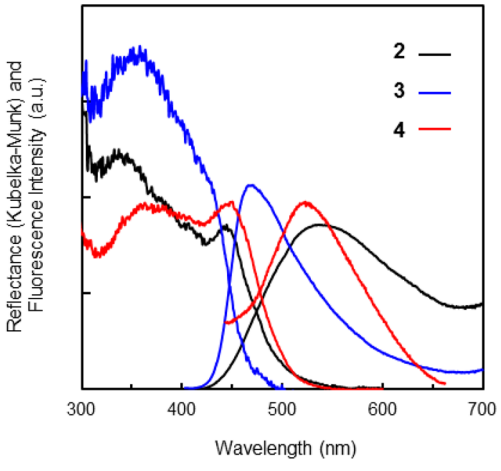

Figure 5. Absorption and fluorescence spectra of **2**–**4** in the solid state. Excitation wavelength: λ_{ex} = 360 nm.

Table 5. Absorption and Fluorescence Data of 2–4 in the Solid State[a]

	2	3	4
λ_a[b]	445 (2.25 × 10^4)	431 (2.32 × 10^4)	450 (2.22 × 10^4)
λ_f[c]	535 (1.87 × 10^4)	469 (2.13 × 10^4)	525 (1.90 × 10^4)
ΔE_{ss}[d] (cm^{-1})	3.8 × 10^3	1.9 × 10^3	3.2 × 10^3
ϕ_f[e]	0.007	0.015	0.003
τ_s[f] (ns)	0.29 (63%), 1.3 (37%)	1.5 (100%)	0.06 (62%), 1.4 (38%)
$\langle\tau_s\rangle$[g] (ns)	0.67	1.5	0.55
k_f[h] (s^{-1})	1.0 × 10^7	1.0 × 10^7	5.4 × 10^6
k_{nr}[i] (s^{-1})	1.5 × 10^9	6.5 × 10^8	1.8 × 10^9

[a]In the microcrystalline state. [b]Absorption maxima in nm. Values in parentheses are in cm^{-1}. [c]Fluorescence maxima in nm. Values in parentheses are in cm^{-1}. Excitation wavelength: λ_{ex} = 360 nm. [d]Stokes shifts calculated from λ_a and λ_f. [e]Fluorescence quantum yields. Excitation wavelength: λ_{ex} = 360 nm. [f]Fluorescence lifetimes. Excitation wavelength: λ_{ex} = 365 nm. Emission (monitor) wavelength: $\lambda_{em} = \lambda_f$. [g]Intensity weighted mean lifetimes. [h]Radiative rate constants: $k_f = \phi_f/\langle\tau_s\rangle$. [i]Nonradiative rate constants: $k_{nr} = (1-\phi_f)/\langle\tau_s\rangle$.

The fluorescence spectrum of **3** is less broad than those of **2** and **4**. The spectrum of **4** has a long tail to the blue and the one of **2** a long tail to the red. This might suggest some differences in the emissive species for **2** and **4**; however, we have no explanation for this at present. The fluorescence spectra shift to longer wavelengths in the following order, **3** → **4** → **2**. For **2** and **4**, λ_f are observed at clearly longer wavelengths than that for **3**. The energy differences in λ_f for **2**–**4** are larger in the solid state than in solution. As a result of this, the red shifts in λ_f on going from solution to the solid state are larger for **2** and **4** than for **3** (Tables 4 and 5). The fluorescence excitation spectrum of **3** is fundamentally the same as the absorption spectrum, and independent of λ_{em}. The fluorescence excitation spectrum of **3** is presented in Figure S9 (Supporting Information).[67]

The fluorescence decay curve of **3** is reasonably fitted by monoexponential function to give τ_s of 1.5 ns (Table 5). The τ_s values of 1–2 ns are similar to those obtained for the other ring-substituted DPHs we reported previously.[20,23] Although we used a thick microcrystalline sample of **3**, it showed simple, monoexponential decay behavior.[68] This strongly suggests that the fluorescence emission from **3** is of monomeric origin. The relatively small red shift in λ_f on going from solution to the solid state and somewhat narrow spectral shape of the solid-state spectrum are also consistent with this assignment. In contrast, the decay behavior of **2** and **4** is much more complex than that of **3**. The decay curves are basically multiexponential and at least two τ_s components are required to give a reasonable fit (Table 5). The values of τ_s at different λ_{em} are summarized in Table S6 (Supporting Information). The complex decay behavior, the relatively large red shifts in λ_f on going from solution to the solid state, and the broad spectral shapes suggest that the fluorescence of **2** and **4** originates from excimers or excimeric species.[1,10] The values of k_f and k_{nr} in the solid state are calculated from $k_f = \phi_f/\langle\tau_s\rangle$ and $k_{nr} = (1-\phi_f)/$

dx.doi.org/10.1021/cg5009363 | Cryst. Growth Des. 2014, 14, 4781–4789

$\langle\tau_s\rangle$, where $\langle\tau_s\rangle$ is the intensity weighted mean lifetime (Table 5). The values of k_f are all small for **2**−**4**, suggesting the forbidden nature of the fluorescence transition in the solid state.

3. Excimer Formation in the Solid State. As described above, the origin of the solid-state fluorescence is shown to be monomeric for **3** and excimeric for **2** and **4**. In each crystal, the stacking molecules are aligned along their long axes (Figures 1−3). Also, the transition dipole moments responsible for the emission processes are predicted to point along the long molecular axes in all three molecules (SI Figure S8). Thus, the molecules of **2**−**4** form 'H-aggregates' (cofacial or π-stack) in the crystals. This is consistent with the small k_f in the solid state (Table 5).

In Table S7 (Supporting Information), we compare the nearest-neighbor cofacial arrangements in the crystals of **2**−**4**, the intermolecular distance (the distance between the LSPs of the molecules) and the relative displacements along the long and short molecular axes.[8a,69] As clearly seen, the $\pi-\pi$ overlaps (orbital interaction) between the nearest stacking molecules are much larger in **2** and **4** than in **3**. This would give direct evidence for the excimer formation in **2** and **4**.

Our present results can be compared with those previously reported[20,21] for 1,6-di(nitrophenyl)-1,3,5-hexatrienes (**2N-4N**, Chart S1 and Figures S10−S12 in Supporting Information), the nitro counterparts of **2**−**4**; it is suggested that the possibility of excimer formation in the solid state is not determined only by the X-ray determined ground-state geometrical parameters such as distances and dihedral angles between the nearest two molecules. It is likely that the interactions between (or among) molecular orbitals in the ground and excited states, involving a large number of (at least more than two) molecules in the crystals, may also be important in the formation of excimeric species.

CONCLUSIONS

In conclusion, we have described the crystal structures and solid-state emission properties of three kinds of cyano-substituted diphenylhexatrienes, **2**−**4**. In all these crystals, the sp^2-CH···N≡C hydrogen bonds were similarly shown to play an important role in constructing the structures. However, the packing pattern was largely different depending on the position of the cyano substituent, and the resulting molecular arrangement directly affected the fluorescence properties. Thus, a very clear structure−property relationship was observed in the present molecules. It would also be valuable that the existence of the sp^2-CH···N≡C hydrogen bonds in crystals **2**−**4** was spectroscopically evidenced by the fact that the IR peaks due to C≡N stretching vibration shifted to red in the solid state relative to those in solution.

ASSOCIATED CONTENT

Supporting Information

Crystallographic data of **2**−**4** in CIF format; crystal and structure refinement data, major geometrical parameters, intermolecular distances and displacements for the nearest stacking molecules in crystals, ORTEP drawings and crystal packing diagrams of **2**−**4**; absorption, fluorescence, and IR spectroscopic data of **2**−**4** in solution and in the solid state; calculated excitation energies and transition dipole moments of **2**−**4**; discussion of the crystal structure and emission properties of **2N-4N**; full author list for ref 30. This material is available free of charge via the Internet at http://pubs.acs.org. Crystallographic information files are also available from the Cambridge Crystallographic Data Center (CCDC) upon request (http://www.ccdc.cam.ac.uk, CCDC deposition numbers 991992−991994).

AUTHOR INFORMATION

Corresponding Author

*TEL: +81-29-861-6390. FAX: +81-29-861-3029. E-mail: y.sonoda@aist.go.jp.

Notes

The authors declare no competing financial interest.

ACKNOWLEDGMENTS

We thank Electronics and Photonics Research Institute (ESPRIT) and Nanosystem Research Institute (NRI), National Institute of Advanced Industrial Science and Technology (AIST), for financial support. We gratefully acknowledge Dr. J. Sugiyama (NRI, AIST) for his help in performing the single crystal X-ray structure analysis.

REFERENCES

(1) Klessinger, M.; Michl, J. *Excited States and Photochemistry of Organic Molecules*; VCH Publishers, Inc.: New York, 1995.
(2) Winnik, F. M. *Chem. Rev.* **1993**, *93*, 587−614.
(3) Sasabe, H.; Kido, J. *Chem. Mater.* **2011**, *23*, 621−630.
(4) Van Hutten, P. F.; Krasnikov, V. V.; Hadziioannou, G. *Acc. Chem. Res.* **1999**, *32*, 257−265.
(5) Wang, H.; Li, F.; Ravia, I.; Gao, B.; Li, Y.; Medvedev, V.; Sun, H.; Tessler, N.; Ma, Y. *Adv. Funct. Mater.* **2011**, *21*, 3770−3777.
(6) An, B.-K.; Gierschner, J.; Park, S. Y. *Acc. Chem. Res.* **2012**, *45*, 544−554.
(7) Gierschner, J.; Lüer, L.; Milián-Medina, B.; Oelkrug, D.; Egelhaaf, H.-J. *J. Phys. Chem. Lett.* **2013**, *4*, 2686−2697.
(8) (a) Gierschner, J.; Park, S. Y. *J. Mater. Chem. C* **2013**, *1*, 5818−5832. (b) Yoon, S.-J.; Varghese, S.; Park, S. K.; Wannemacher, R.; Gierschner, J.; Park, S. Y. *Adv. Opt. Mater.* **2013**, *1*, 232−237.
(9) Yan, D.; Delori, A.; Lloyd, G. O.; Friščić, T.; Day, G. M.; Jones, W.; Lu, J.; Wei, M.; Evans, D. G.; Duan, X. *Angew. Chem., Int. Ed.* **2011**, *50*, 12483−12486.
(10) Suk, J.; Wu, Z.; Wang, L.; Bard, A. J. *J. Am. Chem. Soc.* **2011**, *133*, 14675−14685.
(11) Sugino, M.; Araki, Y.; Hatanaka, K.; Hisaki, I.; Miyata, M.; Tohnai, N. *Cryst. Growth Des.* **2013**, *13*, 4986−4992.
(12) Gierschner, J.; Ehni, M.; Egelhaaf, H.-J.; Medina, B. M.; Beljonne, D.; Benmansour, H.; Bazan, G. C. *J. Chem. Phys.* **2005**, *123*, 144914.
(13) Oelkrug, D.; Tompert, A.; Gierschner, J.; Egelhaaf, H.-J.; Hanack, M.; Hohloch, M.; Steinhuber, E. *J. Phys. Chem. B* **1998**, *102*, 1902−1907.
(14) Gierschner, J.; Egelhaaf, H.-J.; Mack, H.-G.; Oelkrug, D.; Alvarez, R. M.; Hanack, M. *Synth. Met.* **2003**, *137*, 1449−1450.
(15) Hudson, B.; Kohler, B. *Annu. Rev. Phys. Chem.* **1974**, *25*, 437−460.
(16) Allen, M. T.; Whitten, D. G. *Chem. Rev.* **1989**, *89*, 1691−1702.
(17) (a) Allen, M. T.; Miola, L.; Whitten, D. G. *J. Am. Chem. Soc.* **1988**, *110*, 3198−3206. (b) Trotter, P. J.; Storch. *J. Biochim. Biophys. Acta* **1989**, *982*, 131−139. (c) Zhuang, Z.-P.; Kung, M.-P.; Kung, H. F. *J. Med. Chem.* **2006**, *49*, 2841−2844.
(18) Sonoda, Y.; Kawanishi, Y.; Ikeda, T.; Goto, M.; Hayashi, S.; Yoshida, Y.; Tanigaki, N.; Yase, K. *J. Phys. Chem. B* **2003**, *107*, 3376−3383.
(19) Sonoda, Y.; Goto, M.; Tsuzuki, S.; Tamaoki, N. *J. Phys. Chem. A* **2007**, *111*, 13441−13451.
(20) Sonoda, Y.; Tsuzuki, S.; Goto, M.; Tohnai, N.; Yoshida, M. *J. Phys. Chem. A* **2010**, *114*, 172−182.

(21) Sonoda, Y.; Kawanishi, Y.; Goto, M. *Acta Crystallogr.* **2005**, *E61*, o1200−o1202.
(22) Sonoda, Y.; Shimoi, Y.; Goto, M.; Tohnai, N.; Kanesato, M. *J. Phys. Chem. A* **2013**, *117*, 566−578.
(23) Sonoda, Y.; Goto, M.; Tsuzuki, S.; Tamaoki, N. *J. Phys. Chem. A* **2006**, *110*, 13379−13387.
(24) Sonoda, Y.; Miyazawa, A.; Hayashi, S.; Sakuragi, M. *Chem. Lett.* **2001**, *30*, 410−411.
(25) Sonoda, Y. *Molecules* **2011**, *16*, 119−148.
(26) Pfiffi, D.; Bier, B. A.; Marian, C. M.; Schaper, K.; Seidel, C. A. M. *J. Phys. Chem. A* **2010**, *114*, 4099−4108.
(27) Sonoda, Y.; Kwok, W. M.; Petrasek, Z.; Ostler, R.; Matousek, P.; Towrie, M.; Parker, A. W.; Phillips, D. *J. Chem. Soc., Perkin Trans. 2* **2001**, 308−314.
(28) *APEX II v 2009.9*; Bruker AXS Inc. *SAINT v 7.68A*; Bruker AXS Inc., 2009. *SADABS v 2008/1*, Sheldrick, Bruker AXS Inc.
(29) Sheldrick, G. M. SHELXTL v 2008/4; *Acta Crystallogr.* **2008**, *A64*, 112−122.
(30) Frisch, M. J. et al. *Gaussian 09*, Revision A.02; Gaussian, Inc.: Wallingford, CT, 2009.
(31) (a) Lee, C.; Yang, W.; Parr, R. G. *Phys. Rev. B* **1988**, *37*, 785−789. (b) Becke, A. D. *J. Chem. Phys.* **1993**, *98*, 5648−5652.
(32) Stratmann, R. E.; Scuseria, G. E.; Frisch, M. J. *J. Chem. Phys.* **1998**, *109*, 8218−8224.
(33) Hall, T.; Bachrach, S. M.; Spangler, C. W.; Sapochak, L. S.; Lin, C. T.; Guan, H. W.; Rogers, R. D. *Acta Crystallogr.* **1989**, *C45*, 1541−1543.
(34) Nyburg, S. C.; Faerman, C. H. *Acta Crystallogr.* **1985**, *B41*, 274−279.
(35) Mascal, M. *Chem. Commun.* **1998**, 303−304.
(36) Bosch, E. *Cryst. Growth Des.* **2010**, *10*, 3808−3813.
(37) Mazik, M.; Bläser, D.; Boese, R. *Tetrahedron* **2001**, *57*, 5791−5797.
(38) Steiner, T. *Angew. Chem., Int. Ed.* **2002**, *41*, 48−76.
(39) Nishio, M.; Umezawa, Y.; Honda, K.; Tsuboyama, S.; Suezawa, H. *CrystEngComm* **2009**, *11*, 1757−1788.
(40) Desiraju, G. R. *Angew. Chem., Int. Ed.* **1995**, *34*, 2311−2327.
(41) Desiraju, G. R. *Acc. Chem. Res.* **1996**, *29*, 441−449.
(42) Desiraju, G. R. *Chem. Commun.* **1997**, 1475−1482.
(43) Steiner, T. *Chem. Commun.* **1997**, 727−734.
(44) Nangia, A.; Desiraju, G. R. *Acta Crystallogr.* **1998**, *A54*, 934−944.
(45) Desiraju, G. R. *Acc. Chem. Res.* **2002**, *35*, 565−573.
(46) Fauvet, G.; Massaux, M.; Chevalier, R. *Acta Crystallogr.* **1978**, *B34*, 1376−1378.
(47) Janczak, J.; Kubiak, R. *Acta Crystallogr.* **1995**, *C51*, 1399−1401.
(48) Janczak, J.; Kubiak, R. *J. Mol. Struct.* **2000**, *553*, 157−166.
(49) Guth, H.; Heger, G.; Drück, U. *Z. Kristallogr.* **1982**, *159*, 185−190.
(50) Reddy, D. S.; Panneerselvam, K.; Desiraju, G. R. *Acta Crystallogr.* **1995**, *C51*, 2352−2354.
(51) Reddy, D. S.; Goud, B. S.; Panneerselvam, K.; Desiraju, G. R. *J. Chem. Soc., Chem. Commun.* **1993**, 663−664.
(52) Dhurjati, M. S. K.; Sarma, J. A. R. P.; Desiraju, G. R. *J. Chem. Soc., Chem. Commun.* **1991**, 1702−1703.
(53) Dulmage, W. J.; Lipscomb, W. N. *Acta Crystallogr.* **1951**, *4*, 330−334.
(54) Shallcross, F. V.; Carpenter, G. B. *Acta Crystallogr.* **1958**, *11*, 490−496.
(55) Mahapatra, S.; Azim, Y.; Desiraju, G. R. *J. Mol. Struct.* **2010**, *976*, 200−204.
(56) Langley, P. J.; Hulliger, J.; Thaimattam, R.; Desiraju, G. R. *New J. Chem.* **1998**, *22*, 1307−1309.
(57) Van Rij, C.; Britton, D. *Acta Crystallogr.* **1977**, *B33*, 1301−1303.
(58) Drück, U.; Littke, W. *Acta Crystallogr.* **1978**, *B34*, 3095−3096.
(59) Sonoda, Y.; Goto, M.; Ikeda, T.; Shimoi, Y.; Hayashi, S.; Yamawaki, H.; Kanesato, M. *J. Mol. Struct.* **2011**, *1006*, 366−374.
(60) For oligophenylenevinylenes, it is shown that a proper description of the vibronics requires the inclusion of typically at least three effective coupling modes.[61]
(61) Gierschner, J.; Mack, H.-G.; Lüer, L.; Oelkrug, D. *J. Chem. Phys.* **2002**, *116*, 8596−8609.
(62) Muller, J. M.; Harryvan, D. H.; Verhagen, J. C. D.; Van Ginkel, G.; Van Faassen, E. E. *Chem. Phys.* **1996**, *211*, 413−420.
(63) We should note that small shoulders are observed around 400 nm in the fluorescence spectra of **2**−**4** (Figure 4), as in the spectrum of the unsubstituted DPH. For DPH, the emission occurs from S_1 and S_2 (dual fluorescence), and the shoulder is assigned to the $S_2 \rightarrow S_0$ transition.[15,16]
(64) Kasha, M. *Discuss. Faraday Soc.* **1950**, *9*, 14−19.
(65) Strickler, S. J.; Berg, R. A. *J. Chem. Phys.* **1962**, *37*, 814−822.
(66) In optically dense samples like thick films, powders, or crystals, the intrinsic absorption features are strongly masked by size effects.[7]
(67) Attempted measurements of the excitation spectra of **2** and **4** were unsuccessful, probably due to the low values of ϕ_f.
(68) Polycrystalline solid state samples (especially of stronger H-aggregates) often show nonexponential decays due to multiple deactivation pathways, while small single crystals (with minimized reabsorption) typically decay monoexponentially.[8a]
(69) Curtis, M. D.; Cao, J.; Kampf, J. W. *J. Am. Chem. Soc.* **2004**, *126*, 4318−4328.